



HAL
open science

An exoskeleton controlled by an epidural wireless brain–machine interface in a tetraplegic patient: a proof-of-concept demonstration

Alim Louis Benabid, Thomas Costecalde, Andrey Eliseyev, Guillaume Charvet, Alexandre Verney, Serpil Karakas, Michael Foerster, Aurélien Lambert, Boris Morinière, Neil Abroug, et al.

► To cite this version:

Alim Louis Benabid, Thomas Costecalde, Andrey Eliseyev, Guillaume Charvet, Alexandre Verney, et al.. An exoskeleton controlled by an epidural wireless brain–machine interface in a tetraplegic patient: a proof-of-concept demonstration. *The Lancet Neurology*, 2019, 18, pp.1112 - 1122. 10.1016/S1474-4422(19)30321-7 . hal-03489057

HAL Id: hal-03489057

<https://hal.science/hal-03489057v1>

Submitted on 20 Jul 2022

HAL is a multi-disciplinary open access archive for the deposit and dissemination of scientific research documents, whether they are published or not. The documents may come from teaching and research institutions in France or abroad, or from public or private research centers.

L'archive ouverte pluridisciplinaire **HAL**, est destinée au dépôt et à la diffusion de documents scientifiques de niveau recherche, publiés ou non, émanant des établissements d'enseignement et de recherche français ou étrangers, des laboratoires publics ou privés.



Distributed under a Creative Commons Attribution - NonCommercial 4.0 International License

Authors

Alim Louis Benabid^{1,2}, MD, PhD; Thomas Costecalde¹, PhD; Andrey Eliseyev¹, PhD; Guillaume Charvet¹, Eng; Alexandre Verney^{1,3}, Eng; Serpil Karakas¹, Eng; Michael Foerster¹, Eng; Aurélien Lambert¹, Eng; Boris Morinière^{1,3}, Eng; Neil Abroug^{1,3}, Eng; Marie-Caroline Schaeffer¹, PhD; Alexandre Moly¹, Eng; Fabien Sauter-Starace¹, PhD, Eng; David Ratel¹, PhD; Cecile Moro¹, PhD; Napoleon Torres-Martinez¹, MD, PhD; Lilia Langar^{1,2}, Tech; Manuela Oddoux^{1,2}, MD; Stephane Pezzani^{1,2}, Nurse; Vincent Auboiron¹, Eng; Tetiana Aksenova¹, PhD; Corinne Mestais¹, Eng; Stephan Chabardes^{1,2}, MD, PhD

1 Univ Grenoble Alpes, CEA, LETI, CLIMATEC, F-38000 Grenoble, France

2 CHU Grenoble Alpes, F-38000 Grenoble, France

3 CEA, LIST, DIASI, SRI, F-91191 Gif-sur-Yvette France, France

Research in context

Evidence before this study

A PubMed search was performed using the search terms (“FES” OR “electrical stimulation”) and (“BMI” OR “BCI” OR “brain-machine-interface” OR “brain-computer-interface”), with no language or date restrictions. We particularly looked at studies aiming to improve mobility using wireless, semi-invasive methods, and whole-body neuroprostheses. We found a majority of studies using invasive intracortical recording methods to pilot limited action effectors or using FES (surface or transcutaneous) limited to one limb. A single report on chronic ECoG recording using a wireless implanted commercial BMI for written communication was found. We found no studies that were similar to our present study, either in humans or animal models, which used a complete bilateral BMI chain from a cortical source with a high density of electrodes to robotized neuroprosthesis, self-paced algorithm, and multi-limb activation for long-term follow-up in tetraplegic patients.

Added value of this study

Our study is the first to describe the drive of a four-limb exoskeleton following decoding of EpiCoG data recorded by two fully implanted epidural wireless recorders placed above the functionally located sensorimotor cortices. The current 23-month follow-up demonstrates the feasibility of this technique in tetraplegic patients, a lack of surgical and post-surgical complications, the stability of the high-quality recordings, the efficiency of the high dimensional continuous decoding algorithm software, and the

compatibility with day-to-day use without requirement for recalibration over a long period (more than 1.5 months). The quality and stability of the signal provide performances similar to those with microarrays, in a less invasive system.

Implications of all available evidences

Our results show that EpiCoG-recorded data can be precisely decoded to pilot multi-limb neuroprostheses for tetraplegic patients. The usability of this BCI chain in the laboratory as well as at home, paves the way for extension of this methodology to various environments (domestic, urban, and professional). When some needed major improvements (higher resolution electrode grids, data compression,...) are available, this neuroprosthetic ensemble will reach a satisfactory level of usefulness and a strong potential to improve patients' quality of life. This could be a pre-vision of an exoskeleton acting as a patient-to-environment interface, connecting a handicapped person to the external world, to create a new concept of instrumented handicapped persons.

INTRODUCTION

Following cervical spinal cord injury (SCI), approximately 20% of individuals experience complete tetraplegia¹. The degree of sensorimotor deficit depends on the type of spinal cord lesion. Therapeutic approaches aim to restore mobility and improve quality of life. Current studies successfully use neuroprosthetics Brain-computer interfaces (BCI) to bypass the spinal lesion, using functional electrical stimulation of the muscles^{2,3} or of the spinal cord in animals⁴ or humans⁵, or using motorized neuroprostheses and others effectors in humans⁶⁻⁹. Fragments of exoskeleton (hand orthosis^{10,11}, arm¹², lower limbs exoskeleton¹³) have been reported using ElectroEncephaloGraphy (EEG) based BCI for rehabilitation¹¹, or neurological recovery¹³ of patients with severe motor impairment caused by stroke¹¹ or SCI (tetraplegic¹⁰ or paraplegic¹³ patients). Effectors can be controlled by trigger signals from residual volitional functions or brain electrical activity^{7,14-17}, using penetrating microelectrodes¹⁸ or extracerebral grids¹⁹.

Cortical activity has been used to drive effectors since 1998^{6,11,14}. However, despite impressive demonstrations of high dimensional control using wire microelectrode recordings¹⁶, short-term semi-invasive wire ECoG-based BCI with moderate control dimensionality¹⁵, a clinically compatible solution to compensate motor deficits still does not exist.

We designed a program to provide tetraplegic patients with an original neuroprosthesis, driven by the patient's mind, in an unsupervised manner, and fulfilling the requirements of chronically implanted devices (wireless, fully implantable, biocompatible on the long term). The BCI system includes a 64 epidural electrode fully implantable recorder, a 4-limb motorized exoskeleton, embedded decoding algorithms and software. This article presents the first clinical application of this system, and is an

initial report of the clinical trial NCT02550522, focusing on proof of concept in one 2 years followed-up patient, out of 5 patients scheduled.

METHODS

Study Design and Patient

The aim of the study was to evaluate security, long term tolerance and potential benefits of the designed system for tetraplegic patients. The Inclusion Criteria are: Male/female 18-45 years, stability of neurological deficits, need for additional mobility expressed by the patient, ambulatory/hospitalized monitoring, registered in the French social security, signed informed consent. The Exclusion Criteria are: previous brain surgery, anticoagulant treatments, neuropsychological sequelae, depression, substance dependence/abuse, contraindications to MagnetoEncephaloGraphy (MEG), EEG, and Magnetic resonance imaging (MRI).

Two patients were included and operated. In Patient1, at skin closure, the implants were probed, shortly activated, and stopped communicating (details in appendix). The recorders were explanted and Patient1 was excluded from the study. The technical problem was identified, and corrected before Patient2 implantation.

Patient2 was a 28-year-old male, who had tetraplegia following a C4-C5 CSI (Figure 1A). The patient found the link to our clinical trial and spontaneously applied. He was included in the protocol after meeting the criteria and providing written informed consent (by proxy). The participant had little motor control of upper limbs. Real movements were possible only by contraction of biceps (4+ Right, 5 Left) at the elbow, and of extensors of the wrist (0 Right, 3+ Left). All other muscles below were scored 0 (American Spinal Injury Association Impairment Scale, ASIA), not allowing execution of any task. Beyond these muscles, the sensory-motor deficit was complete. He was confined to a wheelchair piloted by a left arm support-joystick and had no other assistive technologies. This patient has been currently followed up for 24 months. There was no adverse effect reported. Three other patients are currently being recruited on the same protocol.

Figure 1

Materials

A new implantable recording system, WIMAGINE®¹⁹, was designed by our team for permanent bilateral epidural implantation over the SMC areas. Electronic components were placed in a titanium case (50 mm diameter, 7-12 mm thick, convex external face). An array of 64 EpiCoG platinum-iridium 90/10 recording electrodes (2 mm in diameter, 4-4.5 mm pitch, five “reference” electrodes) was placed on the flat inner face of the device (Figure 1B). A study on sheep²⁰ demonstrated that EpiCoG recordings remained stable for over eight months. Data were radio-emitted through an ultra-high

frequency (UHF) antenna (402-405 MHz). Power was supplied remotely through a 13.56 MHz inductive high frequency (HF) antenna. Both antennas were embedded in a silicone flap under the temporal muscle. Due to limited data rates, caused by restricted radio link ($\leq 250\text{kb/s}$), only 32 contacts per implant sampled at 586 Hz were used. The wireless connection used 2 external antennas held in front of the recorders by a custom-designed helmet.

The Enhancing Mobility (EMY) exoskeleton (Figure 1C) is a wearable fully motorized four-limb robotic neuroprosthesis (14 joints, 14 actuated Degrees of freedom). It is lightweight (65 kg), designed to be driven by decoded EpiCoG brain signals, completely under the patient's control. The patient was strapped into the exoskeleton, while a back-pack computer station received EpiCoG signals. These signals were decoded in real time and translated into Cartesian position increments for 3D wrist translation and angular increments for 1D wrist rotation. These increments were then sent every 100 milliseconds to the exoskeleton controller, to be translated into motor commands producing anthropomorphic movements of the upper limbs. On the contrary, the activation of the lower limbs was achieved by a switch controlling a humanoid walk program^{21,22}, without equilibrium, requiring ceiling-mounted gravitational compensation.

The paradigms, software, and decoding algorithms were developed and integrated into the Adaptive Brain Signal Decoder (ABSD) framework software²³ to provide adaptive high-resolution decoding of EpiCoG activity within 350 milliseconds, comparable with reaction times measured in normal subjects²⁴. Initially, Recursive Exponentially Weighted N-way Partial Least Squares²³ (REW-NPLS) regression algorithm was the decoder. Switching Markov Linear Model²⁵ (SMLM) was later added to improve decoding stability and resting state support (Timeline, Figure 6).

The subject had permanent access to all Degrees of freedom of the currently used model, and can control any Degrees of freedom at any moment. However, some Degrees of freedoms are kept constant, if the decoder estimates the probability of a subject's intent to activate them as low.

The adaptive decoding algorithms and software (Figure 2 and Figure 3) were developed during a previous preclinical study and tested during a pre-operative MEG-based clinical study (Clinical Trials.gov Identifier: NCT02790411, NCT02790424). The adaptive decoder allows rapid calibration and high-speed online information-decoding (decoder update rate: 0.1-0.06 HZ, control rate: 10 Hz).

Figure 2

Figure 3

Presurgical Targeting and Surgical Procedures

Under MEG and functional MRI (fMRI), the subject performed real or virtual movements with his upper and lower limbs. Each movement was repeated 100 times (random 4-6-second intervals) for

MEG and 80 times (random 10-20-second duration) for fMRI (Clinical Trials.gov Identifier: NCT02574026).

The activities of the SMC neurons during the tasks were detected using a 1.5 T MRI (Espree, SIEMENS) (T1 and T1-Gd sequences for anatomy, and BOLD for Oxygen-dependent changes) (Figure 4A and Supplementary Figure 1), which generated fMRI images (3D SPM graphs) to determine the spatial coordinates of the targets. MEG Images were obtained similarly (Figure 4B and Supplementary Figure 1) using MEG ELEKTA Neuromag 306. Superimposition of fMRI and MEG images outlines the SMC. In addition, MEG signals being non-invasive correlates of ECoG, can be used to check the SMC functionality with the decoders used in the pre-operative procedures.

An Image-Guided Surgiscope® (IGS) (Figure 4F) designated, from fused fMRI-MEG pictures, the putative center of the SMC target as the center of craniotomies.

The electrode grids and the skull were visualized postoperatively by a SIEMENS Symbia Spect CT scanner, providing anatomo-functional correspondence (MRI-CT) coregistration (Figure 4E and Supplementary Figure 1D).

WIMAGINE® recorders are not MEG or MRI compatible, but CT-scans (\pm iodine contrast) can be used whenever needed.

Figure 4

Operative and Post-operative Methods

Surgery was performed under general anesthesia. The IGS neuronavigation software (Figure 4F) was used to bilaterally implant the recorders (Figure 4C and 4D) in front of the SMC. A semi-invasive (as compared to penetrating recording methods) procedure was used (5 cm diameter craniotomy, epidural placement preventing intracranial infections, no electrode penetration of the brain, fully embedded device, completely wireless connections, and even during experiments). The EpiCoG signal was intraoperatively recorded before and after the final skin suture, using an antenna in a sterile bag, to check the lack of implant surgical damage. The recorders are not meant to be explanted, except in case of need.

Outcomes: Cortical recording and Experimental Session Overview

EpiCoG recordings were made for 2 minutes at the beginning of each session to monitor the EpiCoG signal quality (amplitude, SNR, no artifact). BCI tasks were used for calibration, training, and performance/progress evaluation. The participant was asked to mentally 1) trigger an ON/OFF switch or 2) perform a continuous task.

Generally, experiments included two phases: the first being calibration to create or update a decoder and the second being the use of the decoder to estimate its performance. When the performance of a model

is declared as satisfactory, one can reuse it without update for a new session; this has been checked for three different types of experiments during 4, 7, and 7 weeks (Timeline, Figure 6).

The participant mentally triggered ON-OFF events on various effectors, such as “Serious Video Game (SVG) RUNNER” (the subject initiates a manikin walking), an avatar (EMM representing the EMY exoskeleton), or when actually wearing the suspended EMY (walking behavior actuated by an automated 3.5-s walking cycle).

The participant performed a continuous spatial movement of his upper limb segments, combining 3D translations and arm rotations: 1D unidirectional movement (“SVG PONG”: mental control of a paddle to intercept a falling ball), 2D movements (“SVG TARGET” reach-and-touch (on a virtual black panel), or wearing the EMY exoskeleton with fingertip to interact with an 8-LED-panel, on both sides for both arms), 3D and multi-limb movements (using EMM or EMY exoskeleton, facing a panel of 16-LEDs on both sides for both arms), and finally 4D and multi-limb movements (3D displacements plus rotation of the wrist ($\pm 60^\circ$ rotation around arm axis)).

After completing the set of tasks, the subject was challenged to increase the Degrees of freedom for multi-limb mobilization of the two upper limbs (4D each) and lower limbs (switch). The 8D control allowed the participant to perform movements of each arm on free will.

Performance indicators

The subject’s success rates were expressed, for the brain switch (ON-OFF) tasks, as true positive rate ($\text{TPR} = \% \text{ of correct actions} / \text{number of attempts}$), false positives per minute (number of unwanted actions/minute), or false positive rate ($\text{FPR} = \% \text{ of unwanted actions/during rest}$)²⁶. Receiver operating characteristic (ROC) curves and area under curve (AUC) were also calculated (Supplementary Figure 4). For all reach-and-touch sessions, the success rate of reach (percentage of targets hit \pm SD)⁷, as well as the R ratio i.e. the normalized path length of reach (distance traveled from the origin O to the target T by the fingertip versus the actual OT distance) and their change over time (Ratio in Figure 6), was calculated. For each task, the difficulty was kept unchanged throughout the study. Simple statistical analyses, mean and standard deviation (SD), were performed when appropriate. The progress of the patient was investigated in terms of number of Degrees of freedom reached along time (Timeline, Figure 6).

RESULTS

Before the start of this study, the participant was confined to a wheelchair and had very little motor control. However, his fMRI and MEG recordings indicated a good capacity to produce cortical signals when imagining himself performing movements with all his limbs. None of the results presented below indicated a clear improvement, with time or repetition, of the intrinsic performance of the patient for each task. Clinical improvement of the patient’s deficits was neither observed nor expected from this clinical trial.

Immediate post-operative and long-term functionality of the recorders

There was no intraoperative nor postoperative complication during the study. EpiCoG recordings were performed immediately (1 day post-op). This technical test provided proof of the functionality of the entire system. The high signal amplitude ($13.7 \pm 4.47 \mu\text{VRMS}$), which was observed before day 15, increased after resorption of the post-operative serohematic epidural collection ($18.7 \pm 6.54 \mu\text{VRMS}$) from day 30 to day 379. The SNRdB normalized by the bandwidth, (from 34.9 dB for [0;10 Hz] to 4.6 dB for [100;200 Hz]) before day 15, also increased (from 36.5 dB for [0;10 Hz] to 5.0 dB for [100;200 Hz]) from day 30 to day 379 (Figure 1B). The long-term high quality EpiCoG recordings of the SMC allowed the subject to progress through the different learning steps.

To achieve high dimensional control of the exoskeleton, the number of Degrees of freedom was increased gradually from brain switch to 8-Degrees of freedom. The decoder was calibrated/updated regularly. Three special studies to explore the usability of the model without calibration/update during long periods were undertaken, very early in the project for EMM_RUN within 4 weeks, and in more recent experiments 8-Degrees of freedom during 7 weeks controlling either EMM or EMY. The initial decoder was updated twice at 10 and 16 months after surgery (Timeline, Figure 6).

Performance of Brain Switch experiments

In the walking experiments, with the RUNNER the subject achieved $\text{TPR}=82.5 \pm 8.6\%$, $\text{FPR}=12.5 \pm 5.9\%$, and $\text{AUC}=0.78 \pm 0.14$ in 18 experiments; with the EMM Avatar, $\text{TPR}=92.1 \pm 4.3\%$, $\text{FP}=4.9 \pm 1.9/\text{min}$, and $\text{AUC}=0.84 \pm 0.05$ in 15 experiments using the same model without recalibration during one month (Figure 5A, 4C, Video 1). In the ‘Walking the Exoskeleton EMY’ experiment, the patient’s performance was $\text{TPR}=72.6 \pm 15.3\%$, $\text{FP}=7.1 \pm 5.6/\text{min}$, and $\text{AUC}=0.84 \pm 0.06$ over 6 experiments performed just two months post-surgery. The total distance covered was 145 m (480 steps, 39 start-stops, Figure 5A, Video 4). The switch control of the EMM lower limb was also used with success to trigger independent movements of each leg as well as alternating bipedal activity. ROC curves are presented in Supplementary Figure 4.

Performances on Continuous Decoding Experiments

For PONG tasks, involving upper limb control, the patient achieved $54 \pm 12.7\%$ of hits when using his left hand (LH) (19 experiments, Figure 5B, Video 1). In the TARGET task, the subject performed 2D tasks with his LH (17 experiments, $80 \pm 15.5\%$ Hits, ratio 2.8 ± 1.4) (Figure 5C, Supplementary Figure 3A) or with his right hand (RH) (19 experiments, $82.2 \pm 12\%$ Hits, ratio 3.3 ± 1.5) (Figure 5C, Supplementary Figure 3A). In the reach-and-touch experiments with EMM, the patient completed 3D tasks with his LH (7 experiments, $56.9 \pm 15.3\%$ Hits, ratio 6.8 ± 4.1) or RH (11 experiments, $52.5 \pm 11\%$ Hits, ratio 6.6 ± 3.6) (Figure 5D, Supplementary Figure 3B).

The final step in the EMM training/learning program was multi-limb activation of the EMM to generate models that simultaneously controlled several Degrees of freedom in combined tasks. The patient performed 2D-2hands (7 experiments, $69.6 \pm 6.1\%$ Hits, ratio 3.8 ± 1.5) (Figure 5E, Supplementary Figure

3C) and 3D-2hands tasks (6 experiments, $57.2\pm 9.5\%$ Hits, ratio 6.3 ± 3.2) (Figure 5F, Supplementary Figure 3D, Video 2). Finally, the patient successfully performed 8D experiments (3D-2hands and using both hands in pronation/supination). The same model without recalibration was used for all experiments for 7 weeks (11 experiments, 3D-2hands tasks: $64\pm 5.1\%$ Hits, ratio 5.2 ± 1.4 and pronation/supination of both hands: $89.7\pm 5.2\%$ Hits, ratio 5 ± 1.5) (Figure 5G, Supplementary Figure 3E).

Figure 5

In the reach-and-touch experiments with EMY, the patient performed 3D tasks with his LH (2 experiments, $68.9\pm 1.1\%$ Hits, ratio 5.7 ± 2.4) or RH (1 experiment, 61.5% Hits, ratio 6.1 ± 2.5) (Figure 5D, Supplementary Figure 3B).

The final step in the EMY training/learning program was multi-limb activation of EMY to generate models that simultaneously controlled several Degrees of freedom in combined tasks. The patient performed 2D-2hands experiments (1 experiment, 83.8% Hits, ratio 8.4 ± 4.7) (Figure 5E, Supplementary Figure 3C) and 3D-2hands experiments (1 experiment, 71.4% Hits, ratio 5.3 ± 1.4) (Figure 5F, Supplementary Figure 3D). Finally, the patient performed 8D experiments with the same model, without recalibration for over 7 weeks (5 experiments, 3D-2Hands tasks: $70.9\pm 11.6\%$ Hits, ratio 9.8 ± 3.5 and pronation/supination of both hands: $99.2\pm 1.8\%$ Hits, ratio 4 ± 1) (Figure 5G, Supplementary Figure 3E, Video 3). This positive outcome will need to be strengthened in future experiments.

Figure 6

Coherence analysis of achieved movements and involved cortices

The immediate post-operative tangential CT-scan associated the grid contacts with the functional cortices. Using the TFPT paradigm, the patient exerted single-joint movement intentions to show the correspondence between the hand-wrist-finger representation and virtual movements. The extent of cortical activation during virtual movements of the upper limb and lower limb was measured. Lower limb activity correlated with more medial contacts than those related to the upper limb, but still far from the interhemispheric fissure. Movement intentions were associated with neuronal activity detected by EpiCoG and oxygen consumption detected by fMRI. The group of contacts, involved by BCI decoding, colocalized with the EpiCoG and fMRI signals (Supplementary Figure 2D).

DISCUSSION

This paper describes the first successful long-term (24-month) chronic exploitation of bilaterally implanted wireless epidural multi-channel (64) recorders in a paraplegic individual. This is the first time all technical elements (epidural recording, wireless power and emission, online decoding of high number of ECoG channels, and totally embedded) required for long term human clinical application

have been combined. This long-term combination of a large number of bilateral electrodes made it possible to explore multi-limb high dimensional control. Our observation revealed no signal degradation, no side effects, and long-lasting tolerance. This paper reports on the system capacity, using epidural ECoG recorded data, to decode brain activity in a self-paced manner online and in real-time without recalibration for several weeks with no/minimal performance drop.

There was a progressive increase in dimensionality of control from switch (walking experiments) to 8D-bimanual tasks summarized in Figure 6. Results were obtained using subsequent algorithms, starting from an adaptive real time linear decoder to an adaptive real time nonlinear dynamic decoder for multi-limb asynchronous control. This first clinical proof of concept warrants the extension of our system out of the laboratory to a home environment and to other applications.

The successful control of 8-Degrees of freedom (the subject had permanent access to all dimensions), suspended walking during the 24 months following surgical implantation, and continued control after several weeks without recalibration, are the highest performances reported so far in ECoG BCI literature (Figure 6, Figure 5, Supplementary Figure 3). None of the BCI tasks presented here could have been executed by the patient's residual capabilities.

To date, the most performant high-dimensional control (10D control of robotic arm) was reported using invasive microelectrode wire recordings¹⁶. However, chronic applications of such systems are limited due to biocompatibility issues and safety problems, and required further technological developments. In addition, long term (2-5 months) stable switch decoding from LFPs recorded with microelectrodes has been reported in tetraplegic (ALS) patients¹⁷. For higher dimensional control, decoder, usable without re-training several days for 2D cursor control by non-human primates with low/moderate performance drop (~20%-50%) was reported²⁷. In spite of impressive progress, instable calibration still limits clinical application of microelectrode recordings based BCIs. EpiCoG recorders cover a larger cortical surface than do microrecording devices. The invariant spatial positioning of the implant prevents the need for recalibration. The initial goals of our study were met, proving that BCI technologies can involve a high level of sophistication, such as control of a whole-body exoskeleton. The exoskeleton is a biomimetic anthropomorphic neuroprosthesis. It is the potential ultimate solution to totally compensate for the impairment of the quality of a tetraplegic person's life. To date, EMY does not allow autonomous walking with equilibrium. The next goal is to provide a solution for standing displacement of the subject. In the meantime, the demonstration that tetraplegic patients can use their brains to pilot neuroprosthetic effectors, while simultaneously combining several Degrees of freedom, paves the way for extension of this concept to higher-level control. This connection will allow the patient to replace his joystick by conscious control to drive his wheelchair (Video 5). This paves way for progressive integration of the patient in the domestic, urban, and professional environment eventually. The subject already considers his rapidly-increasing prosthetic mobility to be rewarding. However, this, for the moment, has not changed his clinical status. The main goal of this paper is to show that bilateral semi-

invasive epidural chronic implants, driving a four-limb exoskeleton, provide strong perspectives to achieve the expected progress in the field of deficit compensation.

Further studies with these systems will also help us better understand brain function, thanks to the analysis of the cortical events triggered during a task. They will provide information on the roles of the sensorimotor cortex's continued capacity to virtually generate the signals usually needed to achieve real movements (Figure 4, Supplementary Figure 2). Training at home with a researcher (95 days) reinforced the tasks and skills acquired when using EMY at CLINATEC (45 days). In several instances, performance was observed to be better when using EMY than with avatars by an average 10 to 20% increase. This may be due to differences in feedback and subject perception. In the 2D screen projection with EMM, the direct (and sole) feedback is visual, and therefore requires an additional cognitive step to conceptualize the 3rd dimension. In the real 3D environment of EMY, the subject himself is moving in the real world with a richer feedback. The evolution of performances observed throughout the series of experiments raised the question of learning from the subject's point of view. Despite the tendency toward an increase in percentage of hits, as well as a trend for decreasing ratios in the reach-and-touch tasks, it cannot be affirmed that neural changes took place as the model was regularly recreated and the algorithm was improved. Since the 8-Degrees of freedom level has been reached, the model has not changed for 7 weeks; the program for the next period aims to document learning processes during BCI training. Our results suggest that the entire system can accurately harness information from several cortical areas to recreate some degree of assisted mobility in disabled persons. The anatomical and physiological observations are coherent with current knowledge in the field. The hotspots of movement-intention-related EpiCoG activity identified here corresponded to the usual representation on the SMC as described previously by Talairach²⁸, and more recently defined as the Hand Knob by Yousry²⁹. Interestingly, this study might support the hypothesis of training-induced neuroplasticity to develop new functionalities in deafferented unused cortical areas. Although the lower limb representation is buried in the interhemispheric fissure, the most intense lower limb-related EpiCoG activity was often recorded on the most medial contacts of the primary sensory cortex S1. This activity might spread from M1 via transversal intracortical fibers, or from long-distance detection of EpiCoG related to lower limb activity. Alternatively, cortical areas may be recruited by the neighboring motor cortex M1 in response to functional pressure from the prefrontal cortex. This apparent spreading of motor representation over initially sensory cortices might also be related to reports that the motor cortex exhibits sensory responses in a variety of modalities, including vision and somatosensation³⁰. As a result, these studies will provide information on the roles of the sensorimotor cortices from the cortex's continued capacity to generate the signals needed to achieve real or virtual movements (Figure 4, Supplementary Figure 3).

REFERENCES

1. Friggeri A. « Influence du type et du niveau de la lésion, du délai chirurgical et des complications respiratoires sur la récupération clinique à un an » (French). 2006, MD Thesis, Amiens University, France.
2. Bouton CE, Shaikhouni A, Annetta NV, *et al.* Restoring cortical control of functional movement in a human with quadriplegia. *Nature* 2016; **533**(7628): 243–250. doi:10.1038/nature17435.
3. Ajiboye AB, Willett FR, Young DR, *et al.* Restoration of reaching and grasping movements through brain-controlled muscle stimulation in a person with tetraplegia: a proof-of-concept demonstration. *The Lancet*. 2017 **389**(10081). 1821-1830.
4. Capogrosso M, Milekovic T, Borton D, *et al.* A Brain–Spine Interface Alleviating Gait Deficits after Spinal Cord Injury in Primates. *Nature*. 2016; **539**(7628): 284–288. doi:10.1038/nature20118.
5. Mushahwar VK, Guevremont L, Saigal R. Could cortical signals control intraspinal stimulators? A theoretical evaluation. *IEEE Trans Neural Syst Rehabil Eng*. 2006; **14**:198–201. DOI: 10.1109/TNSRE.2006.875532 [PubMed: 16792293].
6. Felton EA, Wilson JA, Williams JC, Garell PC. Electrocuticographically controlled brain-computer interfaces using motor and sensory imagery in patients with temporary subdural electrode implants. Report of four cases. *J Neurosurg*, 2007; **106**:495-500. DOI: 10.3171/jns.2007.106.3.495_
7. Hochberg LR, Bacher D, Jarosiewicz B, *et al.* Reach and grasp by people with tetraplegia using a neurally controlled robotic arm. *Nature*. 2012, **485**(7398). 372.
8. Vansteensel MJ, Pels EGM, Bleichner MG, *et al* Fully implanted brain–computer interface in a locked-in patient with ALS. *N Engl J Med* 2016; **375**:2060-6. DOI: 10.1056/NEJMoa1608085.
9. Taylor DM, Tillery SI, Schwartz AB. Direct cortical control of 3Dneuroprosthetic devices. *Science* **296**, 1829–1832 (2002).
10. Pfurtscheller G, Guger C, Müller G, Krausz G, Neuper C. Brain oscillations control hand orthosis in a tetraplegic. *Neurosci. Lett.* 292(3), 211–214 (2000).
11. Frolov AA, *et al.* Post-stroke Rehabilitation Training with a Motor-Imagery-Based Brain-Computer Interface (BCI)-Controlled Hand Exoskeleton: A Randomized Controlled Multicenter Trial. *Front. Neurosci.* **11**:400 (2017).
12. Donati AR, *et al.* Long-Term Training with a Brain-Machine Interface-Based Gait Protocol Induces Partial Neurological Recovery in Paraplegic Patients. *Sci. Rep.* **6**, 30383 (2016).
13. Elnady AM, Zhang X, Xiao ZG, Yong X, Randhawa BK, Boyd L, Menon C. A Single Session Preliminary Evaluation of an Affordable BCI-Controlled Arm Exoskeleton and Motor-Proprioception Platform. *Front Hum Neurosci*. 2015 Mar 30;**9**:168. doi: 10.3389/fnhum.2015.00168. eCollection 2015.
14. Kennedy PR, Bakay RA. Restoration of neural output from a paralyzed patient by a direct brain connection. *Neuroreport* **9**, 1707–1711 (1998).
15. Wang W, *et al.* An electrocorticographic brain interface in an individual with tetraplegia. *PLoS One*. 2013;**8**(2):e55344. doi: 10.1371/journal.pone.0055344. Epub 2013 Feb 6.

16. Wodlinger B, Downey JE, Tyler-Kabara EC, Schwartz AB, Boninger ML, Collinger JL. Ten-dimensional anthropomorphic arm control in a human brain–machine interface: difficulties, solutions, and limitations. *J. Neural Eng.* **12**(2015) 016011 (17pp).
17. Milekovic T, Sarma AA, Bacher D, *et al.* Stable long-term BCI-enabled communication in ALS and locked-in syndrome using LFP signals. *J Neurophysiol.* 2018 Jul 1; **120**(1):343-360. doi: 10.1152/jn.00493.2017.
18. Simeral JD, Kim SP, Black MJ, Donoghue JP, Hochberg LR. Neural control of cursor trajectory and click by a human with tetraplegia 1000 days after implant of an intracortical microelectrode array *J Neural Eng.* 2011 **8**(2): 025027. doi: 10.1088/1741-2560/8/2/025027.
19. Mestais CS, Charvet G, Sauter-Starace F, Foerster M, Ratel D, Benabid AL. WIMAGINE: Wireless 64-channel EpiCoG recording implant for long term clinical applications. *IEEE transactions on neural systems and rehabilitation engineering.* 2015, **23**(1). 10-21.
20. Cretallaz C, Foerster M, Sauter-Starace F, *et al.* Preclinical chronic implantation of the WIMAGINE® ECoG recording implant: a sheep study. *Neuroscience: S333-02NN6*; Society of Neuroscience, San Diego 2016; 10/2016.
21. Rose J, Gamble JG. (2006). Human walking. ed. *Philadelphia, PA: Lippincott Williams & Wilkins.*
22. Morinière B, Verney A, Abroug N, Garrec P, Perrot Y. "EMY: a dual arm exoskeleton dedicated to the evaluation of Brain Machine Interface in clinical trials," *2015 IEEE/RSJ International Conference on Intelligent Robots and Systems (IROS)*, Hamburg, 2015, pp. 5333-5338. doi: 10.1109/IROS.2015.7354130.
23. Eliseyev A, Auboiroux V, Costecalde T, *et al.* Recursive Exponentially Weighted N-way Partial Least Squares Regression with Recursive-Validation of Hyper-Parameters in Brain-Computer Interface Applications. *Scientific reports* **7.1** (2017): 16281.
24. Kennefick M, Maslovat D, Carlsen AN. The Time Course of Corticospinal Excitability during a Simple Reaction Time Task. *PLoS ONE*, 2014, **9** (11): e113563. doi:10.1371/journal.pone.0113563.
25. Schaeffer MC, Aksenova T. Switching Markov decoders for asynchronous trajectory reconstruction from ECoG signals in monkeys for BCI applications. *Journal of Physiology-Paris.* 2016;110(4), 348-360
26. Eliseyev A, Moro C, Costecalde T, *et al.* Iterative N-way partial least squares for a binary self-paced brain-computer interface in freely moving animals. *J Neural Eng.* 2011 Aug;**8**(4):046012. doi: 10.1088/1741-2560/8/4/046012. Epub 2011 Jun 10. PMID:21659695.
27. Sussillo D, Stavisky SD, Kao JC, Ryu SI, Shenoy KV. Making brain–machine interfaces robust to future neural variability. *Nature communications.* 2016, **7**, 13749.
28. Roux FE, Lotterie JA, Cassol E, Lazorthes Y, Sol JC, Berry I. Cortical areas involved in virtual movement of phantom limbs: comparison with normal subjects. *Neurosurgery.* 2003 Dec;**53**(6):1342-52; discussion 1352-3.

29. Yousry TA, Schmid UD, Alkadhi H, Schmidt D, Peraud A, Buettner A, Winkler P. Localization of the motor hand area to a knob on the precentral gyrus. A new landmark. *Brain* **120**, 141–157 (1997).
30. Hatsopoulos NG, Suminski AJ. Sensing with the Motor Cortex. *Neuron*, 2011 **72**, 477-486.

FIGURES LEGENDS

Figure 1: Clinical data, Recorder and Exoskeleton

A: Clinical data: the subject has no motor control or sensitivity below the red metameric level. The spinal cord lesion is slightly asymmetrical, with more severe deficits (American Spinal Injury Association Impairment Scale, ASIA scores) on the right side (C4: only the biceps and muscles above C5 level are under voluntary control) than on the left side (C5: the subject can contract his biceps, wrist flexors). The sensory map is comparable on both sides (C4). MRI shows extensive severe spinal cord lesion (total atrophy with syringomyelia). The cervical spine has been stabilized with a cage.

B: The biocompatible wireless WIMAGINE® recorder was designed for chronic implantation. It consisted of a titanium case bearing a 64-contact pad on the inner face and two lateral silicone antennae to allow remote HF power supply and UHF transmission of digitized recorded data. A 5 cm diameter craniotomy was performed in front of the target brain region located by fMRI and MEG, and the two implants were placed at a safe distance from the midline (see Figure 4). The portion of the cortex that represents the lower limb is not covered by the recording grid. High quality, stable ECoG recordings were obtained over a period of 24 months. Defining the noise level as the signal between 250 Hz and half the sampling frequency (293 Hz), the SNRdB normalized by the bandwidth is depicted in the table.

C: The EMY Exoskeleton was designed as a wearable humanoid universal neuroprosthesis mimicking the human body shape and its mobility. It is self-supporting, wireless, and autonomous for 2.5 hours. Equilibrated walking is not currently available nor achievable, but it can be achieved with a software that produces a humanoid walk and a ceiling suspension system (Vector Elite model, Bioness. <http://bionessvector.com/vector>). This proof-of-concept prototype will evolve toward lighter, more practicable, and higher-skilled versions.

Figure 2: Real time data processing

A: During the BCI session and task execution (example of single limb target reach), the EpiCoG was simultaneously recorded (32 channels for each WIMAGINE implanted recorder) with the coordinates for hand position and angular wrist rotation, as well as the status of the brain switch for walking. The flow of EpiCoG data was sampled at 586 Hz.

B: During the calibration and training stage, movement features were extracted: vector distance from current hand position (y_1 , y_2 , and y_3 coordinates) to the target position at time t for target reach task, angle between current angular position of the wrist and target angular position at time t for pronation/supination task, and binary variable for walking.

C: complex continuous wavelet transforms (CCWT) (Morlet) were applied to extract EpiCoG features (1 second epoch, 15 frequency bands (range 10-150 Hz) for each channel, 10 times delay with step 0.1 second, absolute value of CCWT averaged in 0.1 second window).

D: A 10-15-second long data stack of extracted features was stored in a temporary buffer along with the data for the movements. This information was used to create the model, which was updated every 10-15 seconds. (The “Updating time” depends on the number of Degrees of freedom: it is 10 seconds for up to 6-Degrees of freedom, but 15 seconds for 8-Degrees of freedom). Intermediate data cumulating necessary information for the update of the model were only stored in running memory with the current 10-15-second long data stack of extracted features during the experiment. Every 0.1 second, an online prediction was made by the current model and corresponding control commands were sent to the effector, using the features extracted from the preceding 1-second recording epoch.

Figure 3

Step 1: Real-time adaptive learning of the model.

Instructions are communicated to the subject (blue arrow), who creates a Mental Task of the Movement, generating neural activity in his SensoriMotor Cortices (SMC). This activity is recorded by WIMAGINE as EpiCoG data which are sent (blue arrow) to the decoder. The ABSD software (Figure 2) analyzes this data and generates commands to drive the motors and move the subject’s or avatar’s limbs. Adaptive model learning and real-time application is used throughout. This process provides the subject with visual feedback (orange arrow), and, only during the calibration phase, provides kinematic feedback to the decoder (orange arrows). Analysis of the initial recording period produces the first decoding model. This model is iteratively updated (every 10-15 second) as the subject performs training tasks. The final model (Fixed Model) can predict task-specific features online and in real-time (within 350 ms). When the prediction is considered adequate, the experimenter terminates building of the model and it is considered ready for use.

Step 2: Using the model.

When the patient creates a new mental task to induce movement, the EpiCoG data generated by his SMC and recorded by WIMAGINE are decoded online in real-time by the Fixed Model. Desired movements are interpreted and commands are generated and communicated to the effectors (e.g. motors of the exoskeleton), which can therefore start moving the limbs accordingly. The resulting action provides visual feedback to the patient allowing him to adjust his mental task when executing the next movement.

Figure 4: Cortical Location of SMC, Targeting, and Surgery

A pre-operative strategy based on fMRI (**A**) and MEG (**B**) was designed to identify the precise surgical target, where recorders should be placed to capture the EpiCoG signatures of the intended movements.

When the patient repeated motor tasks (e.g. real or virtual) metabolic changes were detectable by fMRI (**A**) as BOLD signals. These signals were used to produce task-related functional images visualized using Brainvisa software (3D projections in statistical parametric mode (SPM), Supplementary Figure 1) of the contralateral SMC and ipsilateral cerebellum. Similar MEG images (**B**) were obtained, using the Brainstorm software, for both real (**upper line**) and virtual (**lower line**) flexion of the right and left elbows. fMRI and MEG data from all limb segments were combined; the results were projected onto stereotactic atlas maps and a 3D rendering of the subject's brain. fMRI and MEG data were combined to determine the coordinates of the “hottest” SMC target (white disks, red circles) (C.1), centered near the Rolandic sulcus (**red line**). These coordinates were transferred to the Image-Guided SurgiScope IGS (**D.1**).

According to Penfield's homunculus, the 4x4 cm ECoG grid covers the cortical primary motor **M1** and sensory **S1** functional areas controlling the upper limb (C.2), but not the lower limb (located in the interhemispheric fissure). Photographs taken during the surgical procedure showed placement of implants before closing (**D.2 bottom line**); post-operative X-rays showed their final positions (**D.2 upper line**) at distance from the SLS (superior longitudinal sinus) on the midline.

Figure 5: Cumulative Results of Motor Tasks (also see Figure 6, Supplementary Figure 3 and Videos 1,2,3,4)

A, B: 1D Tasks were performed by activating a switch (**A**) (RUNNER, EMM Avatar, or EMY exoskeleton) or as a 1D displacement (**B**) (PONG horizontal axis).

For the switch triggering the initiation of walking (RUNNER, EMM, EMY), the results can be classified into true positive activation (Blue curve: true positive rate, TPR, as a percentage of positive responses versus the number of intended activations) and random false (unrelated to intentions) positive activation (Red Curve: FPR (false positive rate) for RUNNER or FP/min for EMM and EMY). Graphs corresponding to the results are listed in Figure 6, and plotted as a function of the Experiment number (horizontal axis).

For the 1D horizontal displacement (PONG), the success was estimated based on the percentage of hits when the falling ball was intercepted by the paddle (blue curve, vertical axis) and the number of the falling ball (Red curve, vertical axis).

C: 2D Tasks involved using the hand (R or L) to reach for eight targets on a square in a virtual representation at home (Dark Target). The 2D Graphs show the real cumulated trajectories during one experiment, with left or right hands, and the number of targets reached over the number presented.

D: 3D Tasks involved using the hand (R or L) to reach for 16 targets on a cube in a virtual representation (EMM at Home) or on a solid interface (EMY at CLINATEC). The 3D Graphs show the real cumulated trajectories during one experiment, with left or right hands, and the number reached over the number presented.

E: Multi-limb 4D Tasks involved using both hands (R and L) to reach for eight targets on two flat panels in a virtual representation (EMM at Home) or on a real model (EMY at CLINATEC). The 2D Graphs show the actual trajectories cumulated during one experiment, with left and right hands, and the number of targets reached over the number presented.

F: Multi-limb 6D Tasks involved using both hands (R and L) to reach for 16 targets on two cubes in a virtual representation (EMM at Home) or on a real model (EMY at CLINATEC). The 3D Graphs show the actual trajectories cumulated during one experiment, with left and right hands, and the number of targets reached over the number presented.

G: Multi-limb 8D Tasks involved using both hands (R and L) to reach for 16 targets on two cubes in a virtual representation (EMM at Home) or on a real model (EMY at CLINATEC). This task was performed with the same settings as for 6D + prono-supination of the wrist ($\pm 60^\circ$), which add 1-Degree of freedom per hand. The 3D Graphs show the actual trajectories cumulated during one experiment, with left and right hands, and the number of targets reached over the number presented.

Figure 6

Timeline: Evolution of the number of Degrees of freedom over a period of 20 months (continuous black line), dotted black line indicates the pursuit of experiments not included in the paper (20-24 months). Labels for the ABSD update are shown (red dot). During the 10th month, the initial algorithm REW-NPLS was combined with MSLM. At the 16th month, the parameters were modified for high dimensional control. Periods of no recalibration experiments are depicted (blue line for EMM_RUN, green line for EMM 8D, and orange line for EMY 8D).

Results for detection, model, execution, and performance

Review of performance levels attained in the various training situations:

Upper part: Walking, initiated by switch, using SVG RUNNER, EMM Avatar, and EMY exoskeleton. Data show the number of tests, duration of calibration (per session), duration of the period of full BCI control (per session), true positive rates, and false positive rates or number of false positive events per minute.

Lower part: performance with the right (R) - and left (L) - hand of the upper limbs, using Target for 2D-LH or RH

For TARGET, EMM was used in the subject's home; EMY could only be used at CLINATEC, and thus less frequently. For both EMM and EMY, tasks were performed from 3D to 8D. Data show the number of tests, duration of calibration (per session), duration of the period of full BCI control (per session), and the number of targets, percentage of hits and ratio. The figure illustrates the ratio of the distance traveled, d_T , by the effector from the origin to reach the target over the real origin-to-target distance d_{OT} . In a perfect case, the ratio would be 1. The cut-off time for ending the attempt is when R (ratio) is approximately 30.

Authors contribution

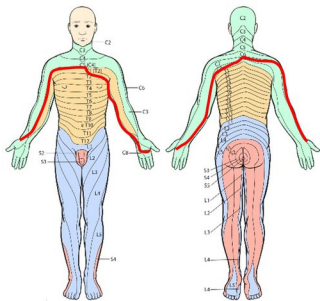
GC, SK, AE Algorithm and Software implementation TA, AE, SK, AM, MCS. BCI system: GC, FSS, MF, AL, AV, BM, NA. Functional Imaging: VA, LL. Performed the experiments: TC, GC, SK, SP Data Analysis and Interpretation: ALB. TC, TA, GC, SK. Surgical design and implementation: SC, ALB, MO. Post-surgical care: SC. SP Wrote the manuscript ALB. TC, TA, Contributed to the writing of the manuscript: GC, FS, MGG (Maighed Gallagher Gambarely Native English Reader) Preclinical experiments: TC, CMO, NTM, DR

Declarations and Conflicts of Interest

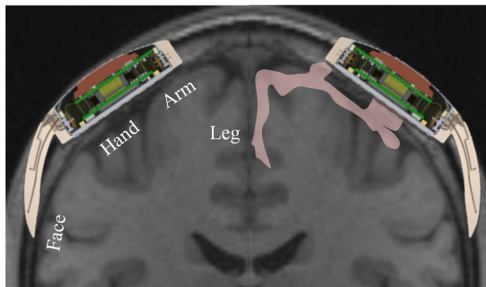
No author has any declarations or conflicts of interest to report.

All authors had complete access to the data. All authors authorized submission of the manuscript, but the final submission decision was made by ALB (primary and corresponding author).

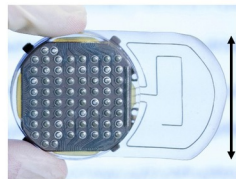
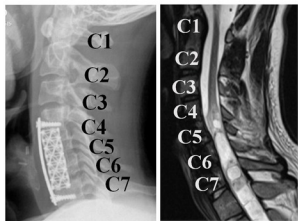
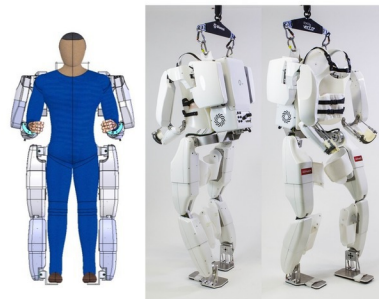
A Clinical Data, XRays and MRI



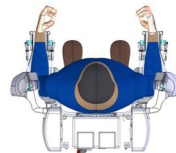
B Wireless recorder Wimage

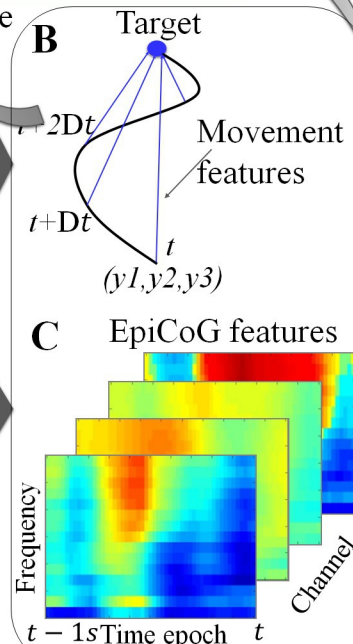
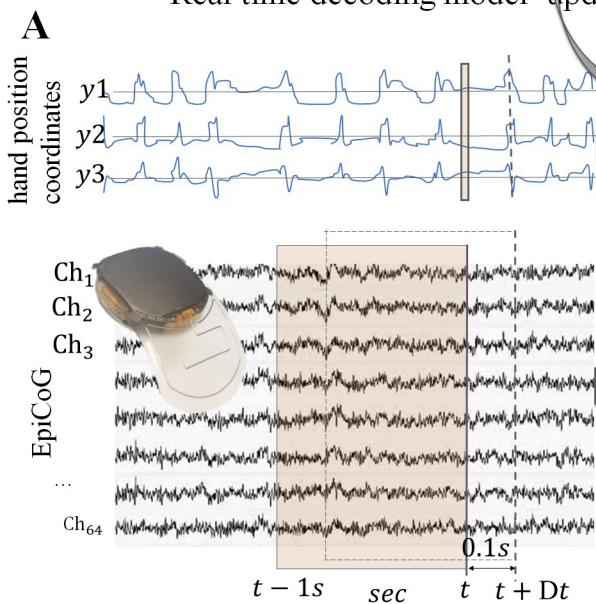
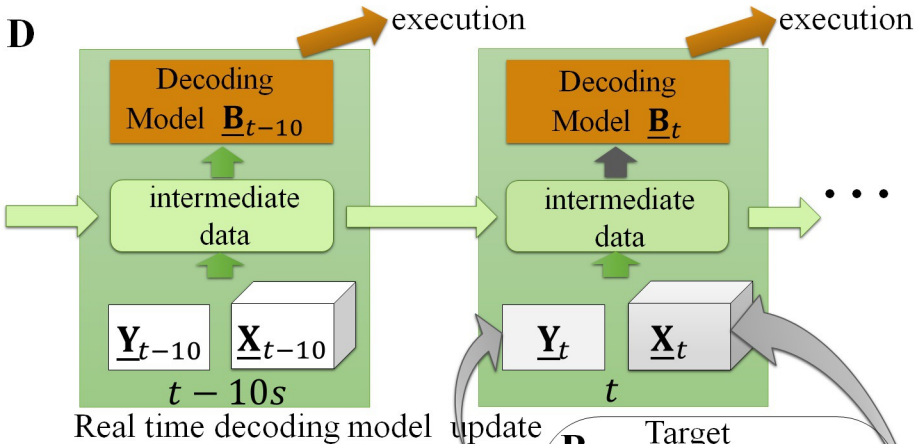


C EMY Exoskeleton

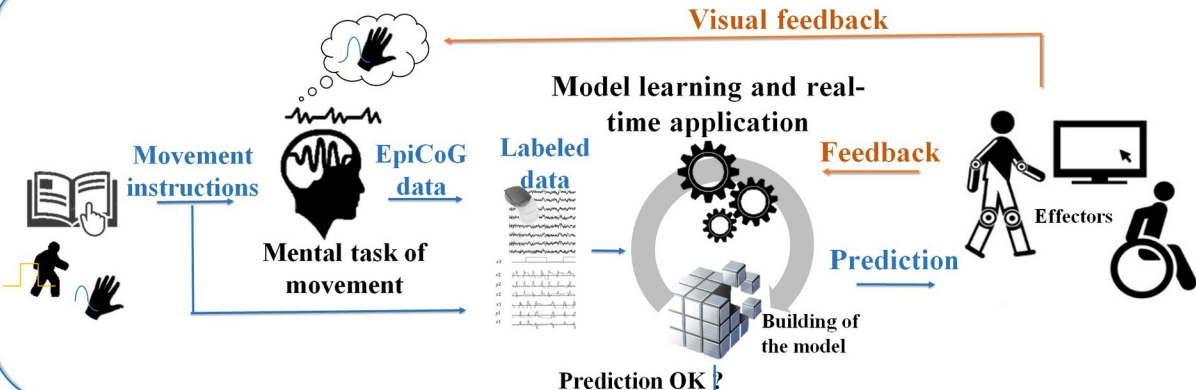


5cm

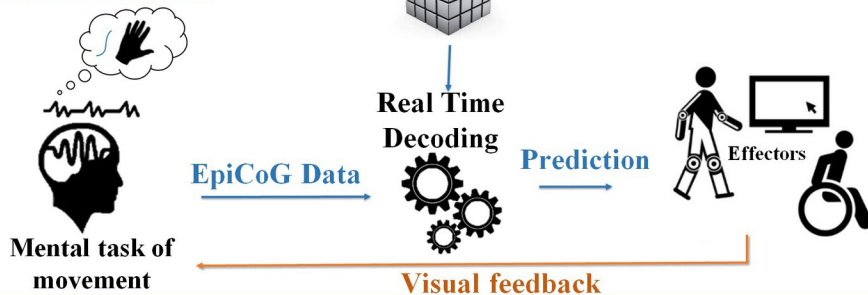




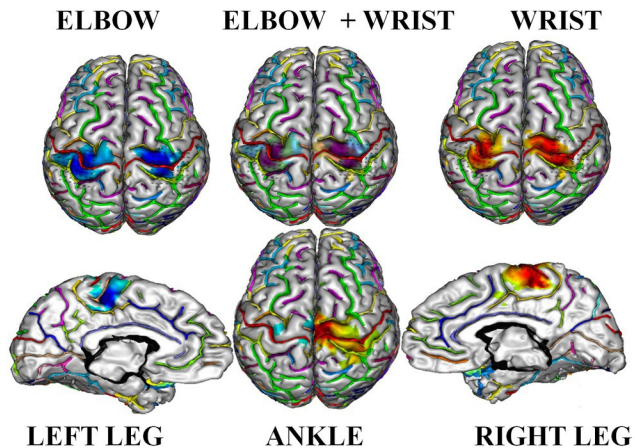
Step 1: Real-time adaptive learning of the model



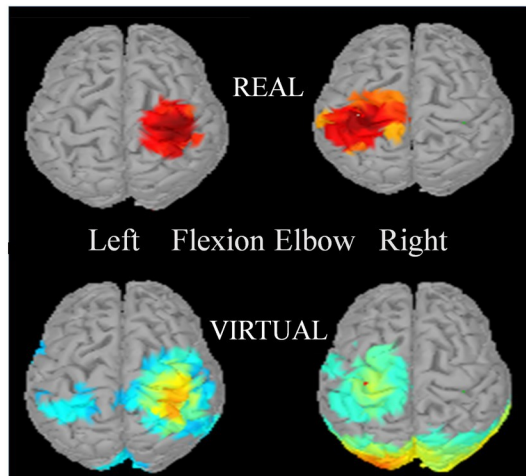
Step 2: Using of the model



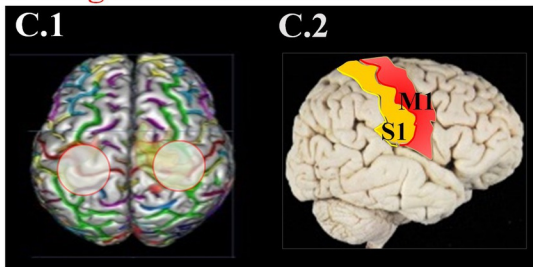
A fMRI # Metabolism



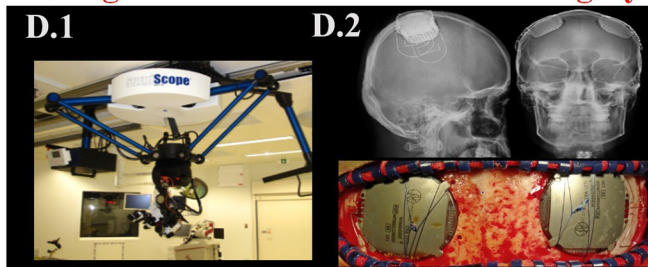
B MEG # ECoG



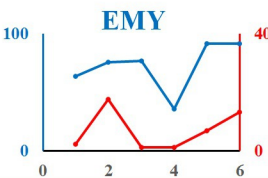
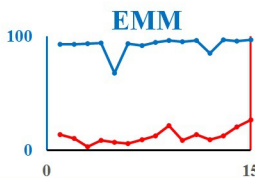
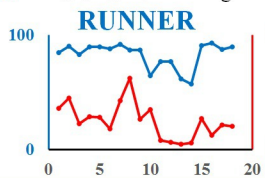
C Target Stereotactic Coordinates



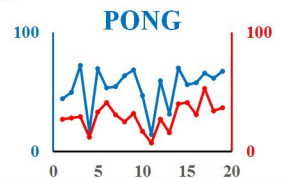
D Image Guided Functional NeuroSurgery



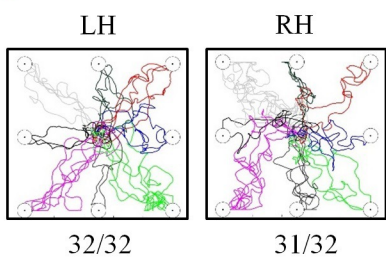
A 1D Switch: Walking Activation



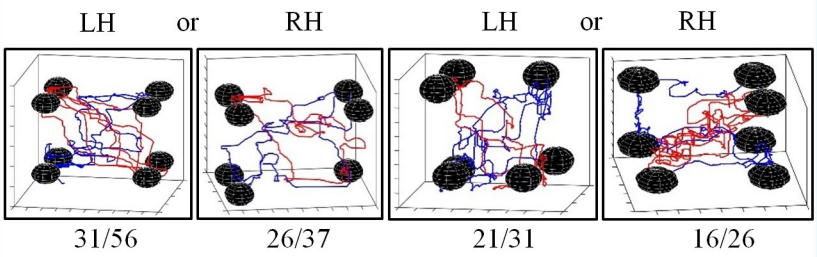
B 1D Movement: Horizontal Y



C 2D Movement: XY

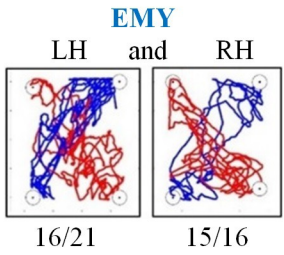
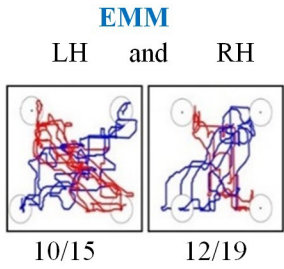


D 3D Movement : XYZ

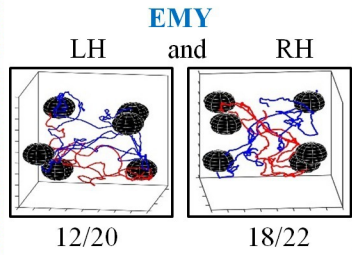
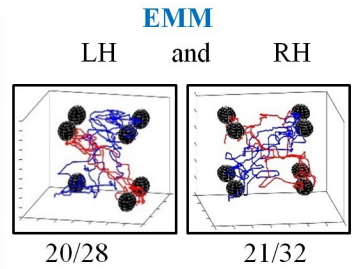


MultiLimb (4D, 6D and 8D)

E 4D (2 arms YZ)



F 6D (2 arms XYZ)



G 8D (2 arms XYZ + 2 arms pronosupination)

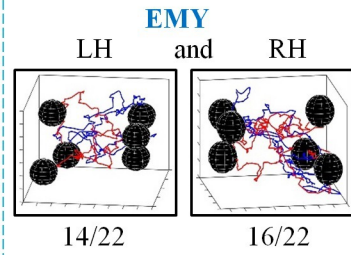
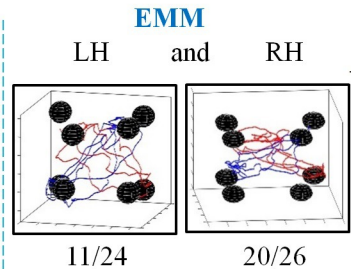
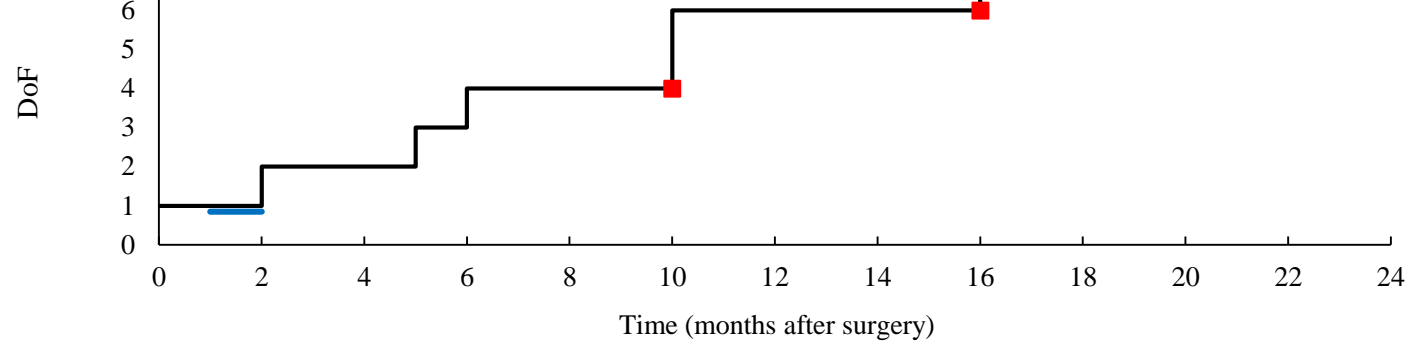
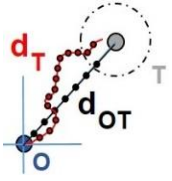


FIGURE 6



- EMM_RUN (1D switch) No Recalibration
- EMM_3D_2H_PRONO (8D) No Recalibration
- EMY_3D_2H_PRONO (8D) No Recalibration

Task	DoF	Number of Experiments	Calibration Duration (minutes)	BMI control Duration (minutes)	TPR (%)	FPR (%) or FP/min	
RUNNER_RUN	1	18	4.2 ± 0.7	5.2 ± 1.6	82.5 ± 8.6	$12.5 \pm 5.9 \%$	
EMM_RUN	1	15	No calibration	8.9 ± 1.2	92.1 ± 4.3	4.9 ± 1.9 /min	
EMY_RUN	1	6	6.1 ± 0.3	10 ± 5.7	72.6 ± 15.3	7.1 ± 5.6 /min	
Task	DoF	Number of Experiments	Calibration Duration (minutes)	BMI control Duration (minutes)	Number of Targets	% Hit	Ratio 
TARGET_2D_LH	2	17	7.7 ± 1.3	9.1 ± 2.1	20.1 ± 8.4	80 ± 15.5	2.8 ± 1.4
TARGET_2D_RH	2	19	9.5 ± 2	7.7 ± 3.6	16.8 ± 6	82.2 ± 12	3.3 ± 1.5
EMM_3D_LH	3	7	20.5 ± 4.2	17.2 ± 4.4	31.3 ± 9.5	56.9 ± 15.3	6.8 ± 4.1
EMM_3D_RH	3	11	22.6 ± 2.2	12.2 ± 6.9	23.2 ± 9.5	52.5 ± 11	6.6 ± 3.6
EMM	4	7	27.6 ± 2.2	12.5 ± 2.2	22.2 ± 7.1	50.6 ± 6.1	2.8 ± 1.5